Viscoelastic Modulus Reconstruction Using Time Harmonic Vibrations

Habib Ammari[a], Jin Keun Seo[b] and Liangdong Zhou[b]

[a]*Department of Mathematics and Applications Ecole Normale Supérieure*
  45 Rue d'Ulm, 75005 Paris, France
[b]*Department of Computational Science and Engineering, Yonsei University*
  50 Yonsei-Ro, Seodaemun-Gu, 120-749 Seoul, Korea
  E-mail(*corresp.*): seoj@yonsei.ac.kr
  E-mail: habib.ammari@ens.fr
  E-mail: cse_zhou@yonsei.ac.kr

Abstract. This paper presents a new iterative reconstruction method to provide high-resolution images of shear modulus and viscosity via the internal measurement of displacement fields in tissues. To solve the inverse problem, we compute the Fréchet derivatives of the least-squares discrepancy functional with respect to the shear modulus and shear viscosity. The proposed iterative reconstruction method using this Fréchet derivative does not require any differentiation of the displacement data for the full isotropic linearly viscoelastic model, whereas the standard algebraic inversion method requires at least double differentiation. Because the minimization problem is ill-posed and highly nonlinear, this adjoint-based optimization method needs a very well-matched initial guess. We find a good initial guess. For a well-matched initial guess, numerical experiments show that the proposed method considerably improves the quality of the reconstructed viscoelastic images.

Keywords: inverse problem, viscoelasticity, ill-posed problem, reconstruction formula.

AMS Subject Classification: 35R30; 65N21; 74G75.

1 Introduction

Elastography [18] aims to provide a quantitative visualization of the mechanical properties of human tissues by using the relation between the wave propagation velocity and the mechanical properties of the tissues. During the last three decades, elastography led to significant improvements in the quantitative evaluation of tissue stiffness. The two major elastographic techniques are based on ultrasound and on magnetic resonance imaging [16, 18, 19, 20]. GE Healthcare has recently commercialized magnetic resonance elastography (MRE). Its main use is to assess mechanical changes in liver tissue. The mechanical properties of tissue include the shear modulus, shear viscosity, and compression

modulus [13]. Quantification of the tissue shear modulus *in vivo* can provide evidence of the manifestation of tissue diseases. For centuries, palpation has been widely used to identify tissue abnormalities and estimate the mechanical properties of tissue. Therefore, it is surprising that the concept of remote palpation, which is the remote imaging of tissue stiffness, was first developed only in the late 1980s [8, 11].

Although significant progress has been made in the development of shear modulus imaging technology, problems remain to enhance the image quality of images of local tissue shear viscosity and shear modulus [9,12,14,17,25,27]. This paper focuses on the image reconstruction methods for tissue viscoelasticity imaging. To simplify the underlying inverse problem, the reconstruction of both the shear modulus and shear viscosity are considered under the assumption of isotropic elastic moduli.

This work considers the inverse problem of recovering the distribution of the shear modulus (μ) and shear viscosity (η) from the internal measurement of the time-harmonic mechanical displacement field **u** produced by the application of an external time harmonic excitation at frequency $\omega/2\pi$ in the range $50 \sim 200$Hz through the surface of the subject. Modeling soft tissue as being linearly viscoelastic and nearly incompressible, the displacement **u** satisfies the elasticity equation

$$\nabla \cdot \left((\mu + i\omega\eta)(\nabla\mathbf{u} + \nabla\mathbf{u}^t)\right) + \nabla((\lambda + i\omega\eta_\lambda)\nabla \cdot \mathbf{u}) + \rho\omega^2\mathbf{u} = 0, \qquad (1.1)$$

where ρ denotes the density of the medium, $\nabla\mathbf{u}^t$ is the transpose of the matrix $\nabla\mathbf{u}$, λ is the compression modulus and η_λ is the compression viscosity.

The most widely used reconstruction method is the algebraic inversion method [16]: For any non-zero constant vector **a**,

$$\mu + i\omega\eta = -\frac{\rho\omega^2(\mathbf{a} \cdot \mathbf{u})}{\nabla \cdot \nabla(\mathbf{a} \cdot \mathbf{u})}, \qquad (1.2)$$

which requires the strong assumptions of $\nabla(\mu + i\omega\eta) \approx 0$ (local homogeneity) and $(\lambda + i\omega\eta_\lambda)\nabla \cdot \mathbf{u} \approx 0$ (negligible pressure).

The algebraic formula (1.2) ignores reflection effects of the propagating wave due to abrupt changes of $\mu + i\omega\eta$, so that the method cannot measure any change of $\mu + i\omega\eta$ in the direction of **a** [12, 22].

To deal with these fundamental drawbacks in the algebraic inversion method, the shear modulus decomposition algorithm based on Helmholtz-Hodge decomposition was developed in [12]. This is a much better performing method; however, it continues to neglect pressure by using $(\lambda + i\omega\eta_\lambda)\nabla \cdot \mathbf{u} = 0$, and is thus not realistic. In [23], the curl operator is applied to the elasticity equation (1.1) to eliminate the troublesome term $(\nabla \times \nabla((\lambda + i\omega\eta_\lambda)\nabla \cdot \mathbf{u}) = 0)$. However, the reconstruction method in [23] requires third-order derivatives of the noisy data **u** which makes it very sensitive to noise in the data. A realistic model must take into account the non-vanishing pressure p [3, 10, 21], which can be defined roughly as $p := \lim_{\lambda \to \infty, \nabla \cdot \mathbf{u} \to 0} (\lambda + i\omega\eta_\lambda)\nabla \cdot \mathbf{u}$.

The shear viscoelasticity reconstruction method proposed in this paper is based on the full elasticity model. It does not require any derivative of **u**. The

minimization of a misfit functional involving the discrepancy between the measured and fitted data is considered. The Fréchet derivatives of the functional with respect to μ and η are then computed by introducing an adjoint problem. This Fréchet derivatives based-iterative scheme requires a well-matched initial guess, because the minimization problem is highly nonlinear and may have multiple local minima. We find a well-matched initial guess that captures the edges of the image of the shear viscoelasticity.

The numerical results presented herein demonstrate the viability and efficiency of the proposed minimization method.

2 Reconstruction methods

2.1 Viscoelasticity model

Let an elastic subject occupy the smooth domain $\Omega \subset \mathbb{R}^d, d = 2, 3$ with boundary $\partial \Omega$. To evaluate the viscoelastic tissue properties, we create an internal time-harmonic displacement in the tissue by applying a time-harmonic excitation through the surface of the object. Under the assumptions of mechanical isotropy and incompressibility in the tissue, the induced time-harmonic displacement at angular frequency ω, denoted by $\mathbf{u}$, is then governed by the full elasticity equation

$$2\nabla \cdot ((\mu + i\omega\eta)\nabla^s \mathbf{u}) + \nabla((\lambda + i\omega\eta_\lambda)\nabla \cdot \mathbf{u}) + \rho\omega^2 \mathbf{u} = 0 \quad \text{in } \Omega, \qquad (2.1)$$

where $\nabla^s \mathbf{u} = \frac{1}{2}(\nabla \mathbf{u} + \nabla \mathbf{u}^t)$ is the strain tensor with $\nabla \mathbf{u}^t$ denoting the transpose of the matrix $\nabla \mathbf{u}$; ρ is the density of the medium; the complex quantity $\mu + i\omega\eta$ is the shear modulus, with μ indicating the storage modulus and η indicating the loss modulus reflecting the attenuation of a viscoelastic medium; λ and η_λ are the compression modulus and compression viscosity, respectively. We assume that these heterogeneous parameters satisfy [13]:

$$\mu > 0, \quad \eta > 0, \quad \eta_\lambda > 0, \quad d\lambda + 2\mu > 0.$$

We denote by H^s the standard Sobolev space of order s and by H_0^s the closure of $\mathcal{C}_0^\infty$, which is the set of $\mathcal{C}^\infty$ compactly supported functions, in the H^s-norm. For a fixed $\epsilon > 0$, denote $\Omega' := \{x \in \Omega \mid \text{dist}(x, \partial\Omega) > \epsilon\}$ and $\mathcal{E} := \Omega \backslash \overline{\Omega'}$. Throughout this paper, we assume that μ and η are contained in the following set

$$\widetilde{S} := \{(\mu_0, \eta_0) + (\phi_1, \phi_2) \mid (\phi_1, \phi_2) \in S\},$$

where positive constants μ_0 and η_0 are respectively known shear modulus and shear viscosity in $\mathcal{E}$. And S is given by

$$S := \{(\phi_1, \phi_2) \in H_0^2(\Omega) \mid c_1 < \phi_1 + \mu_0 < c_2, c_1 < \phi_2 + \eta_0 < c_2,$$
$$\|\phi_j\|_{H^2(\Omega)} \le c_3, \text{ supp } \phi_j \subset \Omega' \text{ for } j = 1, 2\}$$

with c_1, c_2, c_3 being positive constants. Hence, $\tilde{S}$ can be viewed as $\tilde{S} = (\mu_0, \eta_0) + S$.
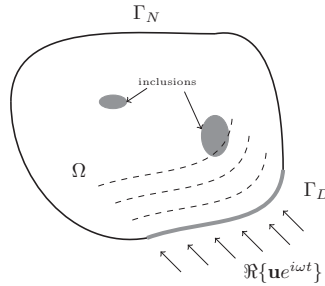
Figure 1. Illustration of the domain and boundary portions.

The domain and boundary portions are shown in Figure 1. To impose boundary conditions, let us take Γ_D and Γ_N such that $\overline{\Gamma_D \cup \Gamma_N} = \partial\Omega$ and $\Gamma_D \cap \Gamma_N = \emptyset$. Typically, we use an acoustic speaker system to generate harmonic vibration. If the acoustic speaker is placed on the portion Γ_D of the boundary $\partial\Omega$, then the boundary conditions for $\mathbf{u}$ can be expressed approximately by

$$\mathbf{u} = \mathbf{g} \qquad \text{on } \Gamma_D,$$
$$2(\mu + i\omega\eta)\nabla^s \mathbf{u}\,\mathbf{n} + (\lambda + i\omega\eta_\lambda)(\nabla \cdot \mathbf{u})\mathbf{n} = 0 \qquad \text{on } \Gamma_N,$$

where $\mathbf{n}$ is the outward unit normal vector to the boundary.

It is known that soft tissues is nearly incompressible and Poisson's ratio ν is close to 0.5 [21]. Therefore, the displacement field $\mathbf{u}$ satisfies $\nabla \cdot \mathbf{u} \approx 0$, and the compression modulus λ fulfills $\lambda = \frac{2\mu\nu}{(1-2\nu)} \approx \infty$. We knew that the term $(\lambda + i\omega\eta_\lambda)\nabla \cdot \mathbf{u}$ in (2.1) is not negligible because $\nabla \cdot \mathbf{u}$ and λ could balance each other out [24]. Let us impose the incompressibility condition $\nabla \cdot \mathbf{u} = 0$. This introduce the internal pressure $p = \lambda\nabla \cdot \mathbf{u}$ which can be understood as a limit of $\lambda\nabla \cdot \mathbf{u}$ as λ goes to infinity and $\nabla \cdot \mathbf{u}$ goes to zero [21]. Then, the time harmonic displacement $\mathbf{u}$ satisfies (approximately) the following quasi-incompressible viscoelasticity model [2, 3]:

$$\begin{cases} 2\nabla \cdot ((\mu + i\omega\eta)\nabla^s \mathbf{u}) + \nabla p + \rho\omega^2 \mathbf{u} = 0 & \text{in } \Omega, \\ \nabla \cdot \mathbf{u} = 0 & \text{in } \Omega, \\ \mathbf{u} = \mathbf{g} & \text{on } \Gamma_D, \\ 2(\mu + i\omega\eta)\nabla^s \mathbf{u}\,\mathbf{n} + p\mathbf{n} = 0 & \text{on } \Gamma_N. \end{cases} \qquad (2.2)$$

We refer the reader to [3, 26] for the reduction of the elasticity equations to the modified Stokes system (2.2). Note that if $\Gamma_D = \partial\Omega$ ($\Gamma_N = \emptyset$), then $\mathbf{g}$ should satisfy the compatibility condition $\int_{\partial\Omega} \mathbf{g} \cdot \mathbf{n}\,ds = 0$. It is worth noticing that p can be regarded as a Lagrange multiplier to enforce the incompressibility condition.

Let $\mathbf{u}_m$ denote the displacement data that is measured in Ω. Then, the inverse problem is to reconstruct the distribution of μ and η from the measured data $\mathbf{u}_m$.

2.2 Optimal control method

Define the misfit (or discrepancy) functional $J(\mu, \eta)$ in terms of μ and η by the L^2-norm in Ω of the difference between the numerical solution $\mathbf{u}[\mu, \eta]$ of the forward problem (2.2) and the measured displacement data $\mathbf{u}_m = \mathbf{u}_m[\mu^*, \eta^*]$:

$$J(\mu, \eta) = \frac{1}{2} \int_\Omega |\mathbf{u}[\mu, \eta] - \mathbf{u}_m|^2 d\mathbf{x}, \qquad (2.3)$$

where μ^* and η^* are true distributions of shear elasticity and viscosity, respectively. The reconstruction of the unknowns μ and η can be obtained by minimizing the misfit functional $J(\mu, \eta)$ with respect to μ and η.

In order to construct a minimizing sequence of $J(\mu, \eta)$, we need to compute the Fréchet derivatives of $J(\mu, \eta)$ with respect to μ and η. Assume that δ_μ and δ_η are small perturbations of μ and η, respectively, by regarding $\frac{\delta\mu + i\omega\delta_\eta}{\mu + i\omega\eta} \approx 0$. For notational simplicity, we denote $\mathbf{u}_0 := \mathbf{u}[\mu, \eta]$, $p_0 :=$ the pressure corresponding to $\mathbf{u}_0$ and $p_0 + p_1 :=$ the pressure corresponding to $\mathbf{u}[\mu + \delta_\mu, \eta + \delta_\eta]$. Denoting the perturbation of displacement field by

$$\delta\mathbf{u} := \mathbf{u}[\mu + \delta_\mu, \eta + \delta_\eta] - \mathbf{u}_0,$$

it follows from (2.2) that

$$2\nabla \cdot ((\mu + i\omega\eta)\nabla^s \delta\mathbf{u}) + \nabla p_1 + \rho\omega^2 \delta\mathbf{u} = -2\nabla \cdot ((\delta_\mu + i\omega\delta_\eta)\nabla^s \mathbf{u}_0)$$
$$- 2\nabla \cdot ((\delta_\mu + i\omega\delta_\eta)\nabla^s \delta\mathbf{u}) \quad \text{in} \quad \Omega. \qquad (2.4)$$

Let $\mathbf{u}_1$ be the solution of the following problem

$$\begin{cases} 2\nabla \cdot ((\mu + i\omega\eta)\nabla^s \mathbf{u}_1) + \nabla p_1 + \rho\omega^2 \mathbf{u}_1 = \\ \qquad\qquad -2\nabla \cdot ((\delta_\mu + i\omega\delta_\eta)\nabla^s \mathbf{u}_0) & \text{in } \Omega, \\ \nabla \cdot \mathbf{u}_1 = 0 & \text{in } \Omega, \\ \mathbf{u}_1 = \mathbf{0} & \text{on } \Gamma_D, \\ 2(\mu + i\omega\eta)\nabla^s \mathbf{u}_1 \mathbf{n} + p_1 \mathbf{n} = 0 & \text{on } \Gamma_N. \end{cases} \qquad (2.5)$$

Now we are ready to state two main theorems in this section which give the Fréchet derivatives of $J(\mu, \eta)$ with respect to μ and η. Denote $\mathbf{A} : \mathbf{B} = \sum_{i,j} A_{ij} B_{ij}$ for two matrices $\mathbf{A} = (A_{ij})$ and $\mathbf{B} = (B_{ij})$.

Theorem 1. *For $(\delta\mu + \mu, \delta\eta + \eta) \in \widetilde{S}$, if $\mathbf{u}_1$ is defined by (2.5), then we have*

$$\Re \int_\Omega \mathbf{u}_1 \overline{(\mathbf{u}_0 - \mathbf{u}_m)} \, d\mathbf{x} = \Re \int_\Omega 2(\delta_\mu + i\omega\delta_\eta)\nabla^s \mathbf{u}_0 : \nabla^s \bar{\mathbf{v}} \, d\mathbf{x}. \qquad (2.6)$$

Furthermore, the Fréchet derivatives of $J(\mu, \eta)$ with respect to μ and η are given by

$$\frac{\partial}{\partial\mu} J(\mu, \eta) = \Re\left[2\nabla^s \mathbf{u}_0 : \nabla^s \bar{\mathbf{v}}\right], \qquad \frac{\partial}{\partial\eta} J(\mu, \eta) = \Re\left[2(i\omega\nabla^s \mathbf{u}_0) : \nabla^s \bar{\mathbf{v}}\right], \qquad (2.7)$$

where the symbol $\Re$ indicates the real part of quantity and $\mathbf{v}$ is the H^1 solution of the following adjoint problem:

$$
\begin{cases}
2\nabla \cdot ((\mu - i\omega\eta)\nabla^s \mathbf{v}) + \nabla q + \rho\omega^2 \mathbf{v} = (\mathbf{u}_0 - \mathbf{u}_m) & in \ \Omega, \\
\nabla \cdot \mathbf{v} = 0 & in \ \Omega, \\
\mathbf{v} = 0 & on \ \Gamma_D, \\
2(\mu - i\omega\eta)\nabla^s \mathbf{v}\,\mathbf{n} + q\mathbf{n} = 0 & on \ \Gamma_N.
\end{cases}
\tag{2.8}
$$

The next theorem shows the differentiability of $J(\mu, \eta)$.

Theorem 2. *The misfit functional $J(\mu, \eta)$ is Fréchet differentiable for $(\mu, \eta) \in \widetilde{S}$. More precisely, if $\mathbf{u}_1 \in H^1(\Omega)$ is the weak solution to (2.5), as the perturbations $\delta_\mu, \delta_\eta \to 0$, we have the following formula:*

$$
\left| J(\mu + \delta_\mu, \eta + \delta_\eta) - J(\mu, \eta) - \Re \int_\Omega \mathbf{u}_1 (\overline{\mathbf{u}_0 - \mathbf{u}_m}) d\mathbf{x} \right|
$$
$$
= O\left((\|\delta_\mu\|_{H^2(\Omega)} + \|\delta_\eta\|_{H^2(\Omega)})^2 \right).
$$

To prove the Fréchet differentiability Theorem 2 and the main Theorem 1, we need the following preliminary results. Firstly, we state an interior estimate for the solution of the Stokes system whose proof basically follows from [5,7,15] by observing $\nabla \cdot \nabla^s \mathbf{w} = \Delta \mathbf{w}$ for $\mathbf{w}$ satisfying $\nabla \cdot \mathbf{w} = 0$.

Lemma 1. *For $\mathbf{F} \in L^2(\Omega)$ and $(\mu, \eta) \in \widetilde{S}$, let $\mathbf{w} \in H^1(\Omega)$ be a weak solution of the following problem:*

$$
\begin{cases}
2\nabla \cdot (\mu + i\omega\eta)\nabla^s \mathbf{w} + \nabla p + \rho\omega^2 \mathbf{w} = \mathbf{F} & in \ \Omega, \\
\nabla \cdot \mathbf{w} = 0 & in \ \Omega, \\
\mathbf{w} = \mathbf{0} & on \ \partial\Omega.
\end{cases}
$$

Then, $\mathbf{w} \in H^2(\Omega)$ and

$$
\|\mathbf{w}\|_{H^2(\Omega)} \leq C \|\mathbf{F}\|_{L^2(\Omega)},
\tag{2.9}
$$

where C is positive constant independent of $\mathbf{F}$.

The following estimate for $\delta\mathbf{u}$ holds.

Proposition 1. *The perturbation of displacement field $\delta\mathbf{u} \in H^1(\Omega)$ satisfies the following estimate:*

$$
\|\delta\mathbf{u}\|_{H^2(\Omega)} \leq C(\|\delta_\mu\|_{H^2(\Omega)} + \|\delta_\eta\|_{H^2(\Omega)}) \|\mathbf{u}_0\|_{H^2(\Omega)},
$$

where C is positive constant independent of δ_μ and δ_η.

Proof.   From (2.4), $\delta\mathbf{u}$ satisfies

$$
2\nabla \cdot ((\mu + \delta_\mu + i\omega(\delta_\eta + \eta))\nabla^s \delta\mathbf{u}) + \nabla p_1 + \rho\omega^2 \delta\mathbf{u}
$$
$$
= -2\nabla \cdot ((\delta_\mu + i\omega\delta_\eta)\nabla^s \mathbf{u}_0) \quad in \quad \Omega.
\tag{2.10}
$$

Applying the interior estimate (2.9) to (2.10) and using Hölder's inequality and Sobolev embedding theorem [1,6], we arrive at

$$\|\delta\mathbf{u}\|_{H^2(\Omega)} \leq C\|\nabla \cdot ((\delta_\mu + i\omega\delta_\eta)\nabla^s\mathbf{u}_0)\|_{L^2(\Omega)}$$
$$\leq C\left(\|\delta_\mu + i\omega\delta_\eta\|_{L^\infty(\Omega)}\|\mathbf{u}_0\|_{H^2} + \|\nabla(\delta_\mu + i\omega\delta_\eta)\|_{L^4(\Omega)}\|\nabla\mathbf{u}_0\|_{L^4(\Omega)}\right)$$
$$\leq C\left(\|\delta_\mu\|_{H^2(\Omega)} + \|\delta_\eta\|_{H^2(\Omega)}\right)\|\mathbf{u}_0\|_{H^2(\Omega)}.$$

This completes the proof. □

Now we are ready to prove Theorem 2.

Proof of Theorem 2: From the definition of $J(\mu, \eta)$ in (2.3), we have

$$J(\mu + \delta_\mu, \eta + \delta_\eta) = J(\mu, \eta) + \Re\int_\Omega \mathbf{u}_1(\overline{\mathbf{u}_0 - \mathbf{u}_m})d\mathbf{x} + \Upsilon,$$

where Υ is

$$\Upsilon = \Re\int_\Omega (\delta\mathbf{u} - \mathbf{u}_1) \cdot (\overline{\mathbf{u}_0 - \mathbf{u}_m})d\mathbf{x} + \frac{1}{2}\int_\Omega |\delta\mathbf{u}|^2 d\mathbf{x}. \qquad (2.11)$$

Using the adjoint problem (2.8), (2.11) can be expressed as

$$\Upsilon = \frac{1}{2}\int_\Omega |\delta\mathbf{u}|^2 d\mathbf{x} + \Re\int_\Omega (\delta\mathbf{u} - \mathbf{u}_1) \cdot (\overline{2\nabla \cdot (\mu - i\omega\eta)\nabla^s\mathbf{v} + \nabla q + \rho\omega^2\mathbf{v}})d\mathbf{x}.$$

Using $\nabla \cdot \delta\mathbf{u} = \nabla \cdot (\mathbf{u}_0 + \delta\mathbf{u}) - \nabla \cdot \mathbf{u}_0 = 0$ and homogeneous boundary conditions for $\mathbf{u}_1$ and $\delta\mathbf{u}$, we have

$$\Upsilon = \frac{1}{2}\int_\Omega |\delta\mathbf{u}|^2 d\mathbf{x} - \Re\int_\Omega (2\nabla \cdot (\delta_\mu + i\omega\delta_\eta)\nabla^s\delta\mathbf{u}) \cdot \bar{\mathbf{v}}d\mathbf{x}.$$

Applying Hölder's inequality, Υ is estimated by

$$|\Upsilon| \leq \frac{1}{2}\|\delta\mathbf{u}\|_{L^2(\Omega)}^2 + (\|\delta_\mu\|_{L^\infty(\Omega)} + \|\omega\delta_\eta\|_{L^\infty(\Omega)})\|\nabla\delta\mathbf{u}\|_{L^2(\Omega)}\|\nabla\bar{\mathbf{v}}\|_{L^2(\Omega)},$$
$$\leq C\|\nabla\delta\mathbf{u}\|_{L^2(\Omega)}\left(\frac{1}{2}\|\nabla\delta\mathbf{u}\|_{L^2(\Omega)} + (\|\delta_\mu\|_{L^\infty(\Omega)} + \|\omega\delta_\eta\|_{L^\infty(\Omega)})\|\nabla\bar{\mathbf{v}}\|_{L^2(\Omega)}\right).$$

Now we apply Proposition 1 to get

$$|\Upsilon| \leq C\left(\|\delta_\mu\|_{H^2(\Omega)} + \|\delta_\eta\|_{H^2(\Omega)}\right)^2 \left(\|\mathbf{u}_0\|_{H^2(\Omega)} + \|\bar{\mathbf{v}}\|_{H^2(\Omega)}\right).$$

The proof is then completed.

Now, it remains to identify the Fréchet derivatives of $J(\mu, \eta)$. According to Theorem 2, the Fréchet derivatives $\frac{\partial}{\partial\mu}J(\mu, \eta)$ and $\frac{\partial}{\partial\eta}J(\mu, \eta)$ can be computed by expressing $\Re\int_\Omega \mathbf{u}_1(\overline{\mathbf{u}_0 - \mathbf{u}_m})d\mathbf{x}$ in terms of δ_μ and δ_η. These are explained in the proof of Theorem 1.

Proof of Theorem 1: We use the adjoint solution $\mathbf{v}$ in (2.8) to get

$$\int_\Omega \mathbf{u}_1 \cdot (\overline{\mathbf{u}_0 - \mathbf{u}_m})d\mathbf{x} = \int_\Omega \mathbf{u}_1 \cdot (\overline{2\nabla \cdot ((\mu - i\omega\eta)\nabla^s\mathbf{v}) + \nabla q + \rho\omega^2\mathbf{v}})d\mathbf{x}. \quad (2.12)$$

Using the vector identity $\nabla \cdot (q\mathbf{u}_1) = \nabla q \cdot \mathbf{u}_1$ and divergence free conditions $(0 = \nabla \cdot \delta\mathbf{u} = \nabla \cdot \mathbf{u}_1 = \nabla \cdot \mathbf{v})$, the identity (2.12) can be rewritten as

$$\int_\Omega \mathbf{u}_1 \cdot \overline{(\mathbf{u}_0 - \mathbf{u}_m)}d\mathbf{x} = -\int_\Omega 2(\mu + i\omega\eta)\nabla^s\mathbf{u}_1 : \nabla^s\bar{\mathbf{v}}d\mathbf{x} + \int_\Omega \rho\omega^2\mathbf{u}_1 \cdot \bar{\mathbf{v}}d\mathbf{x}.$$

Since $\mathbf{u}_1$ satisfies the equation (2.5), we have

$$\int_\Omega \mathbf{u}_1 \cdot \overline{(\mathbf{u}_0 - \mathbf{u}_m)}d\mathbf{x} = \int_\Omega [2\nabla \cdot ((\mu + i\omega\eta)\nabla^s\mathbf{u}_1) + \rho\omega^2\mathbf{u}_1] \cdot \bar{\mathbf{v}}d\mathbf{x},$$

$$= \int_\Omega [-2\nabla \cdot ((\delta_\mu + i\omega\delta_\eta)\nabla^s\mathbf{u}_0) + \nabla p_1] \cdot \bar{\mathbf{v}}d\mathbf{x},$$

$$= \int_\Omega 2(\delta_\mu + i\omega\delta_\eta)\nabla^s\mathbf{u}_0 : \nabla^s\bar{\mathbf{v}}d\mathbf{x}.$$

This proves the formula (2.6). The formula (2.7) can be obtained directly from Theorem 2 and the formula (2.6). This completes the proof.

Based on Theorem 1, the shear modulus and viscosity can be reconstructed by the following gradient descent iterative scheme:

[Step 1] Let $m = 0$. Start with an initial guess of shear modulus μ^0 and shear viscosity η^0.

[Step 2] For $m = 0, 1, \cdots$, compute $\mathbf{u}_0^m$ by solving the forward problem (2.2) with μ and η replaced by μ^m and η^m, respectively. Compute $\mathbf{v}^m$ by solving the adjoint problem (2.8) with $\mu, \eta, \mathbf{u}_0$ replaced by $\mu^m, \eta^m, \mathbf{u}_0^m$, respectively.

[Step 3] For $m = 0, 1, \cdots$, compute the Fréchet derivatives $\frac{\partial J}{\partial \mu}(\mu^m, \eta^m)$ and $\frac{\partial J}{\partial \eta}(\mu^m, \eta^m)$.

[Step 4] Update μ and η as follows:

$$\begin{cases} \mu^{m+1} & = \mu^m - \delta\frac{\partial J}{\partial \mu}(\mu^m, \eta^m), \\ \eta^{m+1} & = \eta^m - \delta\frac{\partial J}{\partial \eta}(\mu^m, \eta^m). \end{cases} \qquad (2.13)$$

[Step 5] Repeat Steps 2, 3, and 4 until $||\mu^{m+1} - \mu^m|| \le \epsilon$ and $||\eta^{m+1} - \eta^m|| \le \epsilon$ for a given $\epsilon > 0$.

2.3 Initial guess

Numerous simulations show that the reconstruction from an adjoint-based optimization method may converge to some local minimum that is very different from the true solution when the initial guess is far from the true solution. We observed that different initial guesses produce different reconstructions, and thus a good initial guess is necessary for accurate reconstruction using the iterative method (2.13).

We examine the optimization method using the initial guess obtained by the direct inversion method (1.2). Numerical simulations with this initial guess

showed that serious reconstruction errors occur near the interfaces of differ- ent materials in the same domain; the direct inversion method cannot probe those interfaces. We found empirically that it is important to find an initial guess capturing the interfaces of different materials for the effective use of the optimization method.

To develop a method of finding such a good initial guess, we adopt the hybrid one-step method [14] which consider the following simplified model ig- noring the pressure term:

$$2\nabla \cdot (\mu + i\omega\eta)\nabla^s \mathbf{u}^\diamond + \rho\omega^2 \mathbf{u}^\diamond \;=\; 0 \quad \text{in } \Omega,$$

where $\mathbf{u}^\diamond$ is regarded as a good approximation of $\mathbf{u}[\mu, \eta]$. To probe the discon- tinuity of $(\mu + i\omega\eta)\nabla^s \mathbf{u}^\diamond$, we apply the Helmholtz decomposition

$$(\mu + i\omega\eta)\nabla^s \mathbf{u}^\diamond = \nabla \mathbf{f} + \nabla \times \mathbf{W} \text{ with } \nabla \cdot \mathbf{W} = \mathbf{0}, \qquad (2.14)$$

where $\mathbf{f}$ and $\mathbf{W}$ are vector and matrix, respectively. The curl of matrix is defined in column-wise sense: $\nabla \times \mathbf{W} = \nabla \times (W_1, W_2, W_3) = (\nabla \times W_1, \nabla \times W_2, \nabla \times W_3)$, where W_j is the j-th column of matrix $\mathbf{W}$ for $j = 1, 2, 3$. Taking dot product of (2.14) with $\nabla^s \mathbf{u}^\diamond$ gives the following formula

$$\mu + i\omega\eta = \frac{\nabla \mathbf{f} : \nabla^s \bar{\mathbf{u}}^\diamond}{|\nabla^s \mathbf{u}^\diamond|^2} + \frac{\nabla \times \mathbf{W} : \nabla^s \bar{\mathbf{u}}^\diamond}{|\nabla^s \mathbf{u}^\diamond|^2}. \qquad (2.15)$$

By taking the divergence to the equation (2.14), we have

$$\Delta \mathbf{f} = -\frac{1}{2}\rho\omega^2 \mathbf{u}^\diamond \quad \text{in } \Omega. \qquad (2.16)$$

By taking the curl operation to the equation (2.14), we have

$$\Delta \mathbf{W} = \nabla \times ((\mu + i\omega\eta)\nabla^s \mathbf{u}^\diamond) \quad \text{in } \Omega. \qquad (2.17)$$

Our proposed method for determining the initial guess is based on the modifying of hybrid one-step method. Using (2.16), an approximation of the vector potential $\mathbf{f}$ corresponding to the measurement $\mathbf{u}_m$ can be computed by

$$\begin{cases} \Delta \widetilde{\mathbf{f}} = -\frac{1}{2}\rho\omega^2 \mathbf{u}_m \quad \text{in } \Omega, \\ \nabla \widetilde{\mathbf{f}} \, \mathbf{n} = (\mu_0 + i\omega\eta_0)\nabla^s \mathbf{u}_m \, \mathbf{n} \quad \text{on } \partial\Omega. \end{cases}$$

On the other hand, $\mathbf{W}$ can not be computed directly from $\mathbf{u}_m$ since (2.17) contains unknown terms μ and η. Regarding $\mu + i\omega\eta$ in (2.17) as $\frac{\nabla \widetilde{\mathbf{f}} : \nabla^s \bar{\mathbf{u}}_m}{|\nabla^s \mathbf{u}_m|^2}$ (see (2.15)), we can compute a rough approximation of $\mathbf{W}$ by solving

$$\begin{cases} \Delta \mathbf{W}_1 = \nabla \times \left(\frac{\nabla \widetilde{\mathbf{f}} : \nabla^s \bar{\mathbf{u}}_m}{|\nabla^s \mathbf{u}_m|^2} \nabla^s \mathbf{u}_m \right) \quad \text{in } \Omega, \\ \mathbf{W}_1 = \mathbf{0} \quad \text{on } \partial\Omega. \end{cases}$$

Similarly, approximating $\mu + i\omega\eta$ by direct inversion formula (1.2), we can compute $\mathbf{W}$ by solving

$$\begin{cases} \Delta \mathbf{W}_2 = \nabla \times \left(-\frac{\rho\omega^2(\mathbf{a}\cdot\mathbf{u}_m)}{\nabla \cdot \nabla(\mathbf{a}\cdot\mathbf{u}_m)} \nabla^s \mathbf{u}_m \right) \quad \text{in } \Omega, \\ \mathbf{W}_2 = \mathbf{0} \quad \text{on } \partial\Omega, \end{cases}$$

where **a** is any nonzero vector.

Now, we use the formula (2.15) to get the initial guess of shear modulus by substituting $\mathbf{f} = \widetilde{\mathbf{f}}$, $\mathbf{W} = (\mathbf{W}_1 + \mathbf{W}_2)/2$ and $\mathbf{u}^\diamond = \mathbf{u}_m$:

$$\mu^0 + i\omega\eta^0 = \frac{\nabla\widetilde{\mathbf{f}} : \nabla^s\bar{\mathbf{u}}_m}{|\nabla^s\mathbf{u}_m|^2} + \frac{\nabla \times (\mathbf{W}_1 + \mathbf{W}_2) : \nabla^s\bar{\mathbf{u}}_m}{2|\nabla^s\mathbf{u}_m|^2}. \tag{2.18}$$

In formula (2.18), the first term provides information in the wave propagation direction while the second term gives the information in the tangent direction of the wave propagation as shown in [14]. Note that if this initial guess is not satisfactory for the adjoint-based optimization problem, one can update the initial guess formula to obtain more accurate one by replacing $(\mu + i\omega\eta)$ in (2.17) by (2.18).

Numerical experiments demonstrates the possibility of probing the discontinuity of the shear modulus effectively. We emphasize that the initial guess plays an important role in Newton's iterative reconstruction algorithm based on the adjoint approach. By observing the adjoint problem (2.8), the load term $\mathbf{u}_0 - \mathbf{u}_m$ is related to the measured data and the initial guess in the first iteration step. If the initial guess ensure that $\|\mathbf{u}_0 - \mathbf{u}_m\|$ is small in certain norm, the iteration scheme will converge and give good results. Otherwise, the initial guess makes $\|\mathbf{u}_0 - \mathbf{u}_m\|$ far from 0 in certain norm, and the iteration scheme may not converge. This will be discussed in Section 3.
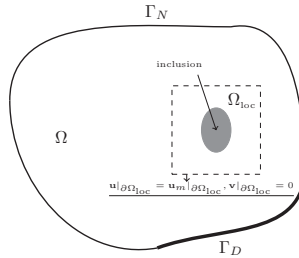
2.4 Local reconstruction

Figure 2. Illustration of the localization of the small anomaly in certain subdomain.

In MRE, the time-harmonic displacement, $\mathbf{u}_m$, in the tissue is measured via phase-contrast-based MR imaging. Hence, the signal-to-noise ratio (SNR) of the data is related to that of the MR phase images, which varies from one region to another. For example, the SNR of data $\mathbf{u}_m$ is very low in MR-defected regions, including the lungs, outer layers of bones, and some gas-filled organs. When the domain, Ω, contains such defected regions, the reconstructed image qualities may be seriously degraded by locally low SNR data in the defected regions. As a result, it would be desirable to exclude defected regions from Ω to prevent errors spreading in the image reconstruction. The illustration is given in Figure 2.

The proposed method is capable of a local reconstruction by restricting to a local domain of the interest. To be precise, let Ω_{loc} be a subdomain of Ω in which $\mathbf{u}_m$ has high SNR. Then, we consider the localized minimization problem

$$J_{\text{loc}}(\mu, \eta) = \frac{1}{2} \int_{\Omega_{\text{loc}}} |\mathbf{u}_{\text{loc}}[\mu, \eta] - \mathbf{u}_m|^2 d\mathbf{x} \qquad (2.19)$$

with $\mathbf{u}_{\text{loc}}[\mu, \eta]$ being the solution of

$$\begin{cases} 2\nabla \cdot ((\mu + i\omega\eta)\nabla^s \mathbf{u}) + \nabla p + \rho\omega^2 \mathbf{u} = 0 & \text{in } \Omega_{\text{loc}}, \\ \nabla \cdot \mathbf{u} = 0 & \text{in } \Omega_{\text{loc}}, \\ \mathbf{u} = \mathbf{u}_m & \text{on } \partial\Omega_{\text{loc}}. \end{cases} \qquad (2.20)$$

As before, we need to compute the corresponding adjoint problem to get Fréchet derivative:

$$\begin{cases} 2\nabla \cdot ((\mu - i\omega\eta)\nabla^s \mathbf{v}) + \nabla q + \rho\omega^2 \mathbf{v} = \mathbf{u}_{0,\text{loc}} - \mathbf{u}_m & \text{in } \Omega_{\text{loc}}, \\ \nabla \cdot \mathbf{v} = 0 & \text{in } \Omega_{\text{loc}}, \\ \mathbf{v} = 0 & \text{on } \partial\Omega_{\text{loc}}. \end{cases} \qquad (2.21)$$

There is no difference between the local reconstruction in Ω_{loc} and the global reconstruction with Ω, except the boundary conditions. As in (2.13), the local reconstruction can be done by solving (2.20) and (2.21) with the initial guess (2.18). Local reconstruction requires that neither the boundary conditions need to be used on the whole domain, Ω, nor that the exact shape of Ω needs to be known. Numerical simulations verify the effectiveness of this local reconstruction, and further discussion will be shown in Section 3.

3 Numerical simulations

In this section, we perform several numerical experiments to illustrate the effectiveness of the shear viscoelasticity reconstruction algorithm proposed in the previous section.

To implement the reconstruction algorithm (2.13) proposed in Section 2, we use the algorithm (2.15) in Section 2.3 to initialize the iteration scheme. For numerical experiments, we set the two dimensional domain as $\Omega = [0, 0.1] \times [0, 0.1]$ m^2 with a boundary denoted by $\partial\Omega = \Gamma_D \cup \Gamma_N$; see Figure 3 (a). We use a finite element method and discretize the rectangular domain Ω into 300×300 triangular elements with linear interpolation functions to solve the forward problem (2.2) as well as the adjoint problem (2.8) at each iteration step in the algorithm (2.13). Fixed iteration step size $\delta = 5 \times 10^6$ is used in the iterative reconstruction algorithm (2.13).

We set three different types of shear viscoelasticity distribution which are shown in the first column of Figure 4, Figure 5 and Figure 6 along with the true distribution of shear modulus and shear viscosity. For each model, the first row shows elasticity while the second row shows viscosity. Our numerical experiments are based on these three models. We generate two dimensional displacements $\mathbf{u}_m = (u_1, u_2)^t$ by solving the problem (2.2) with frequency

$\frac{\omega}{2\pi}$=70Hz and area density $\rho = 1kg \cdot m^{-2}$. We apply the vibration to Γ_D, and the other three sides boundaries are set to be traction free:

$$
\begin{cases}
\mathbf{u} = (0.003, 0.003) & \text{on } \Gamma_D, \\
2(\mu + i\omega\eta)\nabla^s \mathbf{u}\,\mathbf{n} + p\mathbf{n} = 0 & \text{on } \Gamma_N.
\end{cases}
\tag{3.1}
$$

For example, model 1 has the displacement fields shown in Figure 3 where (b) and (c) are real parts of u_1 and u_2, and (d) and (e) are imaginary parts of u_1 and u_2, respectively.

(a) (b) (c) (d) (e)
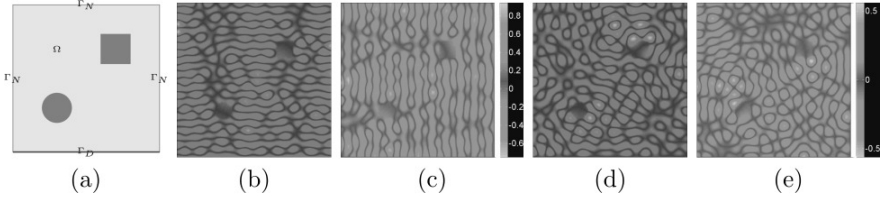
Figure 3. Model 1 and the displacement fields. (a) Model 1; (b) and (c) are real parts of u_1 and u_2; (d) and (e) are imaginary parts of them, respectively.

The next step is to implement our algorithm making use of these displacement fields with certain initial guesses of the distribution of viscoelasticity. We generate the initial guess by the direct inversion method (1.2) shown in the third column of Figures 4, 5 and 6 and the hybrid one-step method (2.15) shown in the fifth column of Figures 4, 5 and 6.
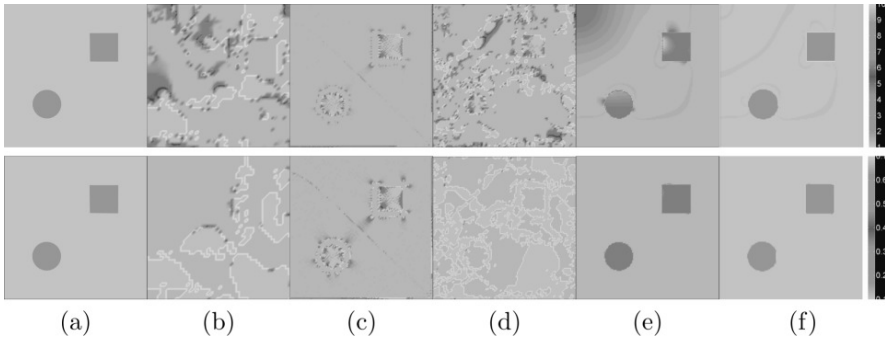

(a) (b) (c) (d) (e) (f)

Figure 4. Case 1: Simulation results for μ (first row) and η_μ (second row) image reconstruction. (a) True images; (c) direct inversion method; (e) hybrid one-step method; (b), (d) and (f) are reconstructed images by the adjoint-based optimization method (2.13) with initial guess of the constant $\mu_0 + i\omega\eta_{\mu_0}$, (c) and (e), respectively.

From the generated initial guess, we can see that the reconstruction by the hybrid one-step method is much better than that of the direct inversion method in catching the inhomogeneous property of the medium. We have already explained the underlying mathematical reason for this phenomenon. We use the initial guesses from these two methods to initialize our proposed

method, and the corresponding numerical results for each model are shown in the fourth column and last column of Figures 4, 5 and 6, respectively. For comparison, we also show the reconstruction with a homogeneous initial guess in each second column of Figures 4, 5 and 6.
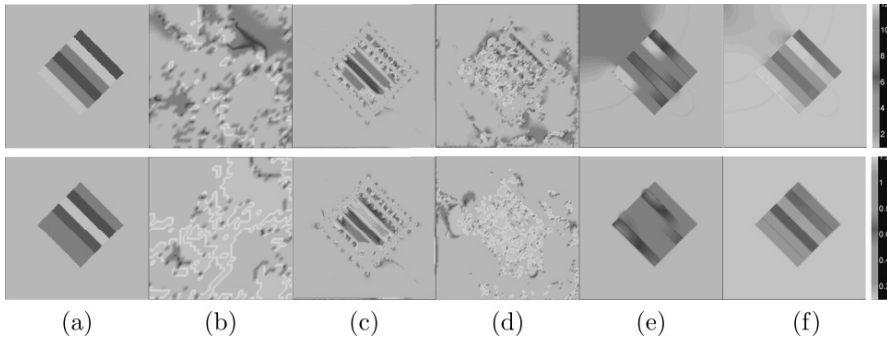

| | | | | | |
| (a) | (b) | (c) | (d) | (e) | (f) |

Figure 5. Case 2: Simulation results for μ (first row) and η_μ (second row) image reconstruction. (a) True images; (c) direct inversion method; (e) hybrid one-step method; (b), (d) and (f) are reconstructed images by the adjoint-based optimization method (2.13) with initial guess of the constant $\mu_0 + i\omega\eta_{\mu_0}$, (c) and (e), respectively.
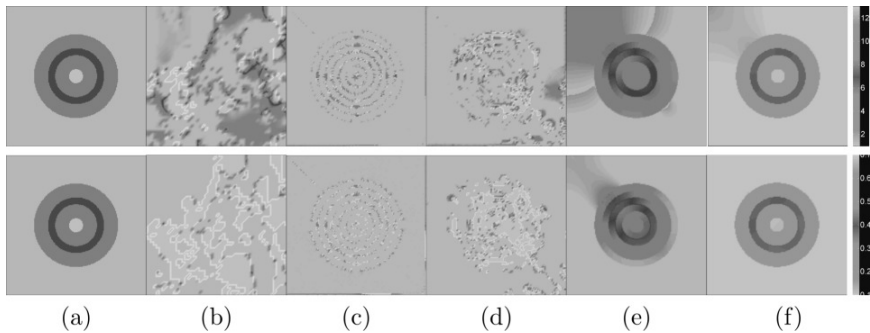

| | | | | | |
| (a) | (b) | (c) | (d) | (e) | (f) |

Figure 6. Case 3: Simulation results for μ (first row) and η_μ (second row) image reconstruction. (a) True images; (c) direct inversion method; (e) hybrid one-step method; (b), (d) and (f) are reconstructed images by the adjoint-based optimization method (2.13) with initial guess of the constant $\mu_0 + i\omega\eta_{\mu_0}$, (c) and (e), respectively.

The reconstruction results (see Figures 4, 5 and 6) show that the proposed method can reconstruct the viscoelasticity distribution with high accuracy (see (f) column) using a well-matched initial guess (see (e) column). Otherwise, poor initial guesses (for example, the homogeneous initial guess and (c)), leads to unsatisfactory reconstructed images (see (b) and (d) columns).

We also numerically evaluate the local reconstruction method proposed in Section 2.4. We consider the rectangular domain, Ω, which is equally divided into four parts: top-left, top-right, bottom-left and bottom-right. It is assumed that the top-right part is contaminated by noise or defected data. For numerical

simplicity, we add 3% white noise to the measured data in the top-right part. The reconstruction results in both the whole domain and the local domains are shown in Figure 7 where (a) is the true distribution of shear viscoelasticity, (b) the initial guess with hybrid method, (c) the reconstruction in whole domain using proposed method, (d) the local reconstruction.
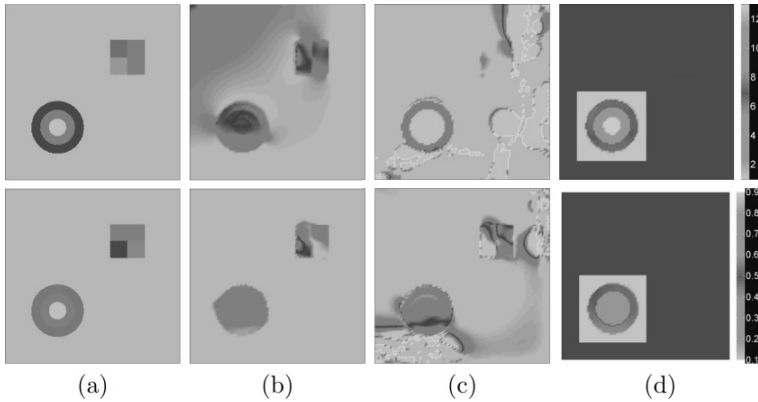

(a)   (b)   (c)   (d)

Figure 7. Simulation results for local reconstruction. First row: images of μ. Second row: images of η_μ. (a) true image; (b) initial guess; (c) adjoint-based optimization method; (d) local reconstruction.

4 Conclusions

In this paper, we propose a reconstruction algorithm for shear elasticity and shear viscosity in a viscoelastic tissue. Our optimization-based approach involves introducing an adjoint problem to avoid taking any derivative of the measured time-harmonic internal data. The proposed initial guess formula is particularly suitable for imaging viscoelastic inclusions. The local convergence of the developed optimal control approach is an open problem. The recent stability results in [4, 28] may be helpful in solving this difficult question. It would be also very interesting to generalize the proposed method for imaging anisotropic viscoelastic media. Another challenging problem is to recognize the disease state in tissue from multifrequency elastographic measurements. These important problems will be the subject of future work.

Acknowledgements

References

[1] R.A. Adams and J.J.F. Fournier. *Sobolev Spaces. Second edition.* Pure and Applied Mathematics, Elsevier/Academic Press, Amsterdam, 2003.

[2] H. Ammari, E. Bretin, J. Garnier, H. Kang, H. Lee and A. Wahab. *Mathematical Methods in Elasticity Imaging.* Princeton Series in Applied Mathematics, Princeton University Press, 2015.

[3] H. Ammari, P. Garapon, H. Kang and H. Lee. A method of biological tissues elasticity reconstruction using magnetic resonance elastography measurements. *Quarterly of Applied Mathematics*, **66**(1):139–176, 2008. http://dx.doi.org/10.1090/S0033-569X-07-01089-8.

[4] H. Ammari, A. Waters and H.Zhang. Stability analysis for magnetic resonance elastography. *Journal of Mathematical Analysis and Applications*, **430**(2):919–931, 2015. http://dx.doi.org/10.1016/j.jmaa.2015.05.029.

[5] Y.Z. Chen and L.C. Wu. *Second order Elliptic Equations and Elliptic Systems.* Translations of Mathematical Monographs, American Mathematical Society, 2004.

[6] L.C. Evans. *Partial Differential Equations. Second edition.* American Mathematical Society, USA, 2010. http://dx.doi.org/10.1090/gsm/019.

[7] M. Giaquinta and L. Martinazzi. *An introduction to the Regularity Theory for Elliptic Systems, Harmonic Maps and Minimal Graphs.* Springer Science & Business Media, 2013.

[8] C.R. Hill, J.C. Bamber and G.R. Haar. *Physical Principles of Medical Ultrasonics. Second Edition.* John Wiley & Sons, 2004. http://dx.doi.org/10.1002/0470093978.

[9] Y. Jiang, H. Fujiwara and G. Nakamura. Approximate steady state models for magnetic resonance elastography. *SIAM Journal on Applied Mathematics*, **71**(6):1965–1989, 2011. http://dx.doi.org/10.1137/100781882.

[10] A. Kozhevnikov. On the first stationary boundary-value problem of elasticity in weighted sobolev spaces in exterior domains of r^3. *Applied Mathematics and Optimization*, **34**(2):183–190, 1996. http://dx.doi.org/10.1007/BF01182623.

[11] T.A. Krouskop, D.R. Dougherty and F.S. Vinson. A pulsed Doppler ultrasonic system for making noninvasive measurements of the mechanical properties of soft tissue. *The journal of Rehabilitation Research and Development*, **24**(2):1–8, 1987.

[12] O.I. Kwon, C. Park, H.S. Nam, E.J. Woo, K.L. Glaser J.K. Seo, A. Manduca and L. Ehman. Shear modulus decomposition algorithm in magnetic resonance elastography. *Medical Imaging, IEEE Transaction on*, **28**(10):1526–1533, 2009. http://dx.doi.org/10.1109/TMI.2009.2019823.

[13] L.D. Landau and E.M. Lifshitz. *Theory of Elasticity. 3rd edition.* Elsevier Butterworth-Heinemann, 1986.

[14] T.G. Lee, C.Y. Ahn, O.I. Kwon and J.K. Seo. A hybrid one-step inversion method for shear modulus imaging using time-harmonic vibrations. *Inverse Problems*, **26**(8), 2010. http://dx.doi.org/10.1088/0266-5611/26/8/085014.

[15] Y.T. Li and L. Nirenberg. Estimates for elliptic systems from composite material. *Communications on Pure and Applied Mathematics*, **56**(7):892–925, 2003. http://dx.doi.org/10.1002/cpa.10079.

[16] A. Manduca, T.E. Oliphant, M.A. Dresner, S.A. Kruse J.L. Mahowald, E. Amromin, J.P. Felmlee, J.F. Greenleaf and R.L. Ehman. Magnetic resonance elastography: Non-invasive mapping of tissue elasticity. *Medical Image Analysis*, **5**(4):237–254, 2001.

[17] J. McLaughlin, A. Oberai and J.R. Yoon. Formulas for detecting a spherical stiff inclusion from interior data: a sensitivity analysis for the Helmholtz equation. *Inverse Problems*, **28**(8), 2012. http://dx.doi.org/10.1088/0266-5611/28/8/084004.

[18] R. Muthupillai, D.J. Lomas, P.J. Rossman, J.F. Greenleaf, A. Manduca and R.L. Ehman. Magnetic resonance elastography by direct visualization of propagating acoustic strain waves. *Science*, **269**(5232):1854–1857, 1995. http://dx.doi.org/10.1126/science.7569924.

[19] T.E. Oliphant, A. Manduca, R.L. Ehman and J.F. Greenleaf. Complex-valued stiffness reconstruction for magnetic resonance elastography by algebraic inversion of the differential equation. *Magnetic Resonance in Medicine*, **45**(2):299–310, 2001. http://dx.doi.org/10.1002/1522-2594(200102)45:2.

[20] E. Park and A.M. Maniatty. Shear modulus reconstruction in dynamic elastography: time harmonic case. *Physics in Medicine and Biology*, **51**(15):3697–3721, 2006. http://dx.doi.org/10.1088/0031-9155/51/15/007/.

[21] A. Sarvazyan, T.J. Hall, M.W. Urban, M. Fatemi, S.R. Aglyamov and B. Garra. An overview of elastography - an emerging branch of medical imaging. *Current Medical Imaging Reviews*, **7**(4):255–282, 2011. http://dx.doi.org/10.2174/157340511798038684.

[22] J.K. Seo and E.J. Woo. *Nonlinear Inverse Problems in Imaging.* John Wiley & Sons, Ltd, Chichester, UK, 2012. http://dx.doi.org/10.1002/9781118478141.

[23] R. Sinkus, M. Tanter, S. Catheline, J. Lorenzen, C. Kuhl, E. Sondermann and M. Fink. Imaging anisotropic and viscous properties of breast tissue by magnetic resonance-elastography. *Magnetic resonance in medicine*, **53**(2):372–387, 2005. http://dx.doi.org/10.1002/mrm.20355.

[24] R. Sinkus, M. Tanter, T. Xydeas, S. Catheline, J. Bercoff and M. Fink. Viscoelastic shear properties of in vivo breast lesions measured by MR elastography. *Magnetic resonance in medicine*, **23**(2):159–165, 2005. http://dx.doi.org/10.1016/j.mri.2004.11.060.

[25] J. Song, O.I. Kwon and J.K. Seo. Anisotropic elastic moduli reconstruction in transversely isotropic model using MRE. *Inverse Problems*, **28**(11), 2012. http://dx.doi.org/10.1088/0266-5611/28/11/115003.

[26] R. Temam. *Navier-Stokes Equations: Theory and Numerical Analysis.* North-Holland Publishing Company, Amsterdam, New York, Oxford, 1977.

[27] D.J.N. Wall, P. Olsson and E.E.W. van Houten. On an inverse problem from magnetic resonance elastic imaging. *SIAM Journal on Applied Mathematics*, **71**(5):1578–1605, 2011. http://dx.doi.org/10.1137/110832082.

[28] T. Widlak and O. Scherzer. Stability in the linearized problem of quantitative elastography. *Inverse Problems*, **31**(3), 2015. http://dx.doi.org/10.1088/0266-5611/31/3/035005.